



Article

# Symmetric Graphene Dielectric Nanowaveguides as Ultra-Compact Photonic Structures

Da Teng <sup>\*,†</sup> , Yuncheng Wang <sup>†</sup>, Tianzi Xu, Huayu Wang, Qinqin Shao and Yanan Tang <sup>\*</sup>

College of Physics and Electronic Engineering, Zhengzhou Normal University, Zhengzhou 450044, China; wyc768020@163.com (Y.W); xu991105@gmail.com (T.X); diandianfeihuayu@163.com (H.W.); scu\_sq@163.com (Q.S)

\* Correspondence: tengda@zznu.edu.cn (D.T.); yntang2010@163.com (Y.T.)

† These authors contributed equally to this work.

**Abstract:** A symmetric graphene plasmon waveguide (SGPWG) is proposed here to achieve excellent subwavelength waveguiding performance of mid-infrared waves. The modal properties of the fundamental graphene plasmon mode are investigated by use of the finite element method. Due to the naturally rounded tips, the plasmon mode in SGPWG could achieve a normalized mode field area of  $\sim 10^{-5}$  (or less) and a figure of merit over 400 by tuning the key geometric structure parameters and the chemical potential of graphene. In addition, results show that the modal performance of SGPWG seems to improve over its circular counterparts. Besides the modal properties, crosstalk analysis indicates that the proposed waveguide exhibits extremely low crosstalk, even at a separation distance of 64 nm. Due to these excellent characteristics, the proposed waveguide has promising applications in ultra-compact integrated photonic components and other intriguing nanoscale devices.

**Keywords:** graphene plasmons; waveguides; subwavelength structures; mid-infrared waves



**Citation:** Teng, D.; Wang, Y.; Xu, T.; Wang, H.; Shao, Q.; Tang, Y. Symmetric Graphene Dielectric Nanowaveguides as Ultra-Compact Photonic Structures. *Nanomaterials* **2021**, *11*, 1281. <https://doi.org/10.3390/nano11051281>

Academic Editor: Detlef W. Bahnemann

Received: 1 April 2021  
Accepted: 10 May 2021  
Published: 13 May 2021

**Publisher's Note:** MDPI stays neutral with regard to jurisdictional claims in published maps and institutional affiliations.



**Copyright:** © 2021 by the authors. Licensee MDPI, Basel, Switzerland. This article is an open access article distributed under the terms and conditions of the Creative Commons Attribution (CC BY) license (<https://creativecommons.org/licenses/by/4.0/>).

## 1. Introduction

Plasmonic waveguides (PWGs) [1], which can confine and guide light at the subwavelength scale, are one of the components necessary to realize ultra-high-density photonic integration [2]. The traditional noble metallic PWGs, such as metal stripe/nanowire waveguides [3–5], channel/wedge plasmon waveguides [6], gap plasmon waveguides [7–9], dielectric-loaded plasmon waveguides [10–12], and hybrid PWGs [1,13–18], have been intensively studied in the near-infrared and visible bands. However, in the mid- and far-infrared bands, the plasmonic effects of metals (which were modeled as perfect electric conductors) are very weak and the electromagnetic optical response cannot be dynamically adjusted, which imposes restrictions on their applications at the nanoscale [19,20]. Thus, finding appropriate materials for PWGs is an urgent need.

To address this critical challenge, researchers have suggested some available materials with tunable properties for exciting surface plasmons [21], including graphene [22–24], transition metal dichalcogenides [25–27], bulk Dirac semimetals [28,29], borophene [30,31], etc. Among these, graphene plasmons (GPs) have attracted widespread attention due to their advantages, including strong light–matter interactions, deep subwavelength field confinement, and tunable optical properties [23,24]. Benefiting from these excellent characteristics, graphene has served as an effective nanoscale waveguiding platform in the infrared region. More importantly, the combination of graphene and silicon-on-insulator (SOI) waveguides make it possible to design graphene-based photonic integration devices [32], such as waveguides [33–39], sensors [40,41], filters [42], modulators [43,44], etc. Recently, graphene–SiO<sub>2</sub>–Si coaxial-like waveguides [45], graphene layer–SiO<sub>2</sub>–Si planar structures [46–50], and graphene-coated nanowires integrated with SiO<sub>2</sub> or Si substrates [51–56] were presented to demonstrate ultra-compact photonic integrated circuits in the mid- and far-infrared bands.

The combination of graphene and silicon-based waveguides not only provides additional degrees of freedom to tune the modal properties, but also leads to strong coupling between the graphene layer and silicon layer, which massively reduces the modal field area. To realize ultra-compact photonic integration, the modal field area should be small enough to circumvent the interference between neighboring structures. Therefore, highly concentrated modal fields are preferred. Here, we propose a symmetric graphene plasmon waveguide (SGPWG) to achieve nanoscale waveguiding of mid-infrared waves. The results of our simulations show that the elliptical nanowire-based SGPWG performs better than its circular counterparts and is suitable for ultra-compact photonics integration. We first introduce the waveguide structure and methods, then comprehensively evaluate the proposed waveguide in the light of geometric and physical parameters. We also discuss the dependences of modal properties on the ratio of the semi-major axis to the semi-minor axis. Finally, we present the crosstalk analysis and briefly compare the mode characteristics of the elliptical nanowire-based SGPWG with those of the circular nanowire-based SGPWG.

## 2. Waveguide Structure and Methods

Figure 1 shows the schematic of the proposed SGPWG, which is composed of two graphene-coated elliptical nanowires symmetrically placed on each side of a thin Si slab with a small gap distance,  $h$ . The semi-minor axis and semi-major axis of the elliptical nanowire are  $a$  and  $b$ , respectively. The thickness and width of the Si slab are  $H$  and  $W$ , respectively. The relative permittivities of the dielectric nanowire, Si slab, and surrounding silica are set as  $\epsilon_1 = 2$ ,  $\epsilon_2 = 12.25$  (with an approximated refractive index of 3.5), and  $\epsilon_3 = 2.25$ , respectively [57–59]. The dielectric nanowires are coated by the monolayer graphene. In this work, the monolayer graphene is simulated as an electric field-induced surface current ( $\mathbf{J} = \sigma_g \mathbf{E}$ ) on the nanowire surfaces [60]. Graphene's surface conductivity ( $\sigma_g$ ) is obtained from Kubo's formula, which consists of the intra- and inter-band contributions [56], namely  $\sigma_g = \sigma_{\text{intra}} + \sigma_{\text{inter}}$ , where:

$$\sigma_{\text{intra}} = \frac{2ie^2k_B T}{\pi\hbar^2(\omega + i/\tau)} \ln[2 \cosh(\frac{E_F}{2k_B T})] \quad (1)$$

$$\sigma_{\text{inter}} = \frac{e^2}{4\hbar} \left[ \frac{1}{2} + \frac{1}{\pi} \arctan\left(\frac{\hbar\omega - 2E_F}{2k_B T}\right) - \frac{i}{2\pi} \ln \frac{(\hbar\omega + 2E_F)^2}{(\hbar\omega - 2E_F)^2 + (2k_B T)^2} \right] \quad (2)$$

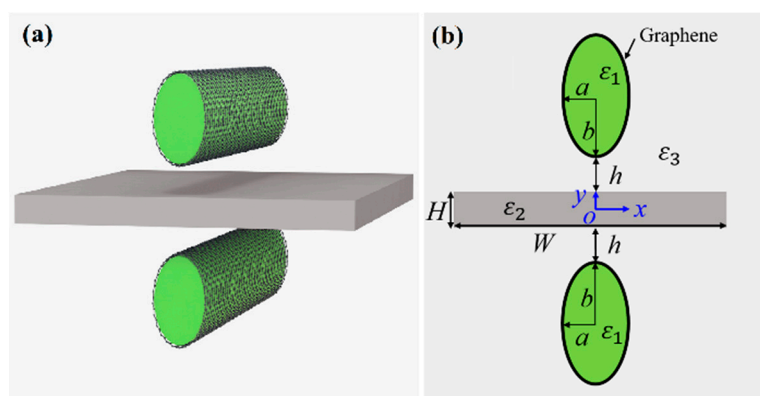


**Figure 1.** Schematic of the proposed SGPWG. (a) Three-dimensional (3D) view, (b) two-dimensional (2D) cross-section.

The electron relaxation time  $\tau$  is set at 0.5 ps according to [61]. The temperature is  $T = 300$  K;  $\omega = 2\pi f$ , with  $f$  being the frequency of the incident light;  $E_F$  is the chemical potential;  $\hbar$  is the reduced Planck's constant;  $k_B$  is the Boltzmann's constant; and  $e = 1.6 \times 10^{-19}$  C.

The GP mode propagates along the  $z$ -direction with a complex propagation constant  $k_z$ , where:  $k_z = k_0 N_{\text{eff}}$ ;  $k_0 = 2\pi/\lambda_0$ , where  $\lambda_0$  is the wavelength in air; and  $N_{\text{eff}}$  is the complex effective mode index. The propagation distance is calculated by  $L_P = \lambda_0/[2\pi\text{Im}(N_{\text{eff}})]$ , where  $\text{Im}(N_{\text{eff}})$  denotes the imaginary part of  $N_{\text{eff}}$ . The normalized mode size is defined as  $A_N = A_{\text{eff}}/A_0$ , where  $A_0 = \lambda_0^2/4$ , and  $A_{\text{eff}}$  is defined as

$$A_{\text{eff}} = \iint W(\mathbf{r})d^2\mathbf{r}/\max\{W(\mathbf{r})\} \quad (3)$$

where  $W(\mathbf{r})$  represents the energy density of the plasmon mode [1]. Figure of merit (FoM) [62] is defined as  $L_P/(A_{\text{eff}}/\pi)^{1/2}$ . The modal properties are investigated by the finite element method (FEM) software COMSOL Multiphysics, which is capable of precisely modeling complex plasmonic structures and thus widely used [1,60,63].

### 3. Results and Discussion

The time-averaged Poynting vector along the  $z$ -direction is given as  $S_z = 1/2\text{Re}(\mathbf{E} \times \mathbf{M}^*)|_z$ , where  $\text{Re}(\cdot)$  is the real part, the superscript of  $\mathbf{M}$  is the complex conjugate, and  $\mathbf{E}$  and  $\mathbf{M}$  are the electric and magnetic field vectors. Figure 2a–c depicts the 2D energy density ( $S_z$ ) distributions of the fundamental mode in SGPWG for different gap distances ( $h = 2, 5, 10$  nm), where  $a = 50$  nm,  $b = 100$  nm,  $W = 400$  nm,  $H = 20$  nm,  $E_F = 0.5$  eV, and  $f = 30$  THz. It could be seen that the optical energy of the plasmon mode is mainly concentrated between the nanowire and the Si layer. For  $h = 2, 5$ , and 10 nm, the peak values of the energy density are 0.36, 0.13 and 0.06  $\text{W}/\text{m}^2$ , respectively. To get an intuitive view, Figure 2d,e depicts the normalized energy density distributions along the  $x$  (at  $y = 0$  nm) and  $y$  (at  $x = 0$  nm) directions (shown in Figure 1b), respectively. Clearly, the energy is mainly restricted between the nanowires. With increasing  $h$ , the field confinement weakens, and the energy density becomes more dispersed. Both features are consistent with the coupling behavior between metal nanoparticles [64]. This is because the coupling strength between the GP mode and silicon layer decreases when  $h$  increases. In order to increase the degree of field confinement, the gap should be at the deep subwavelength scale (e.g., 2~20 nm), which in turn can help to avoid crosstalk between optical signals in the photonic integrated circuits.

As elliptical nanowires are involved in the proposed SGPWG, we need to consider different  $b/a$  values. We chose four representative  $b/a$  values throughout the paper, namely  $b/a = 0.5, 1, 2$ , and 5. Although the case of  $b/a = 1$  has already been investigated in [52], we show that the  $b/a > 1$  setting presented an increased subwavelength optical energy transmission performance as compared to the  $b/a = 1$  setting.

Figure 3 shows the relationship between the fundamental mode properties and the gap distance  $h$  at different  $b/a$  values ( $b/a = 0.5, 1, 2$ , and 5). The parameters were  $a = 50$  nm,  $W = 400$  nm,  $H = 20$  nm,  $E_F = 0.5$  eV, and  $f = 30$  THz. From Figure 3a, it can be seen that the real parts of the effective mode indices ( $n_{\text{eff}}$ ) decrease with the increase in  $h$  for  $b/a = 0.5, 1, 2$ , and 5. For the case of  $b/a = 0.5$ , the coupling between the plasmon mode and the Si layer is much stronger, and then gradually weakens with the increase in  $b/a$ . For the four cases considered here,  $L_P$  increases with the increase in  $h$ . As a whole, the propagation distance also increases with the increase in  $b/a$ , as shown in Figure 3b. Figure 3c,d shows the normalized mode area and figure of merit, respectively. As stated above, the smaller the gap distance, the better the field confinement. Therefore, one can see that  $A_N$  varies from  $3.76 \times 10^{-6}$  to  $8.305 \times 10^{-5}$  when  $h$  increases from 2 to 12 nm. At a fixed  $h$  value, the normalized mode area decreases with the increase in  $b/a$ . Finally, the plots of figure of merit shown in Figure 3d indicate that the overall performance of the SGPWG can be improved when  $h$  is reduced.

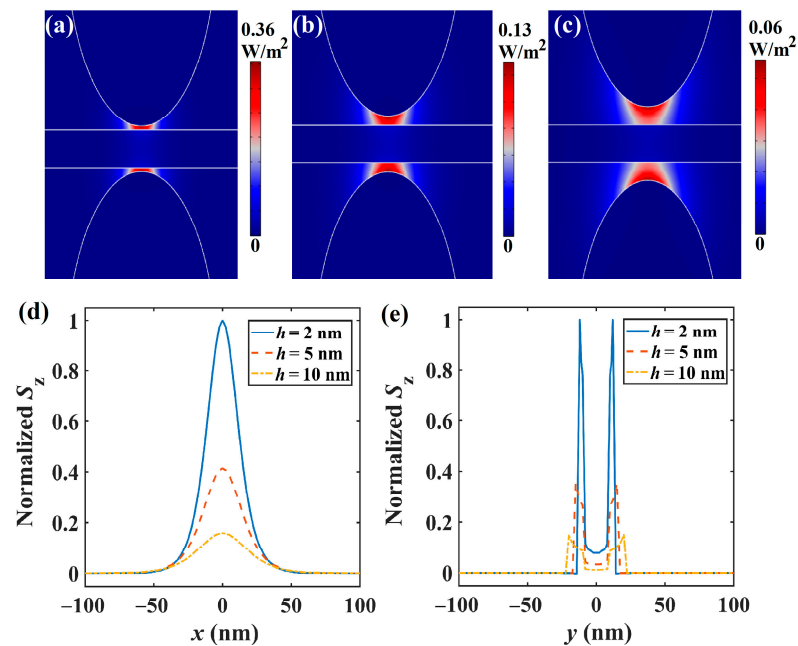


**Figure 2.** Energy density distribution. (a–c) Two-dimensional energy density distributions when  $h = 2, 5,$  and  $10$  nm. (d–e) Normalized energy density distributions along the  $x$  (at  $y = 0$  nm) and  $y$  (at  $x = 0$  nm) directions (shown in Figure 1b).

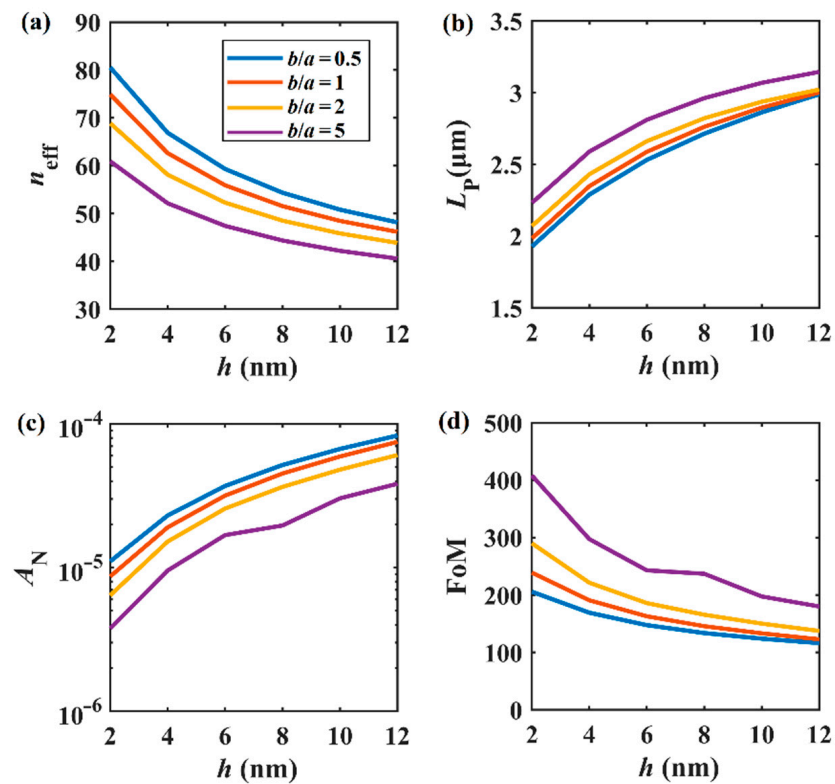


**Figure 3.** Modal properties of  $h$  at different  $b/a$  values. (a)  $n_{\text{eff}}$ , (b)  $L_P$ , (c)  $A_N$ , (d) FoM.

Based on above simulations, we show that the cases of  $b/a > 1$  (orange and purple lines) show better performances compared with the cases of  $b/a = 1$  (red lines) and  $0.5$  (blue lines) in terms of  $L_P$ ,  $A_N$ , and FoM. In other words, these results show that the modal

performance of elliptical nanowire-based SGPWG is better than its circular counterparts. Noticing that the FoM decreases with the increase in the gap distance  $h$ , we set  $h = 5$  nm in the following experiments to maintain the good performance of this structure.

Figure 4 shows the relationship between the fundamental mode properties and the thickness of the silicon layer at  $b/a = 0.5, 1, 2,$  and  $5$  when  $a = 50$  nm,  $W = 400$  nm,  $h = 5$  nm,  $E_F = 0.5$  eV, and  $f = 30$  THz. The modal properties are similar to those presented in Figure 3, except for Figure 4b, where the propagation length seems to have a maximum value when  $H$  is around 30 nm. As shown in Figure 4b,c, when  $H$  increases,  $L_P$  first reaches a maximum value and then slightly decreases, while the normalized mode area  $A_N$  increases monotonically. With increasing  $H$ , the corresponding effective mode index and FoM decrease significantly, as shown in Figure 4a,d. Hence, we set  $H = 20$  nm to maintain a large FoM value in the following experiments. Apparently,  $b/a > 1$  settings (orange and purple lines) perform better than  $b/a = 1$  (red lines) and  $0.5$  (blue lines) settings in terms of  $L_P$ ,  $A_N$ , and FoM.

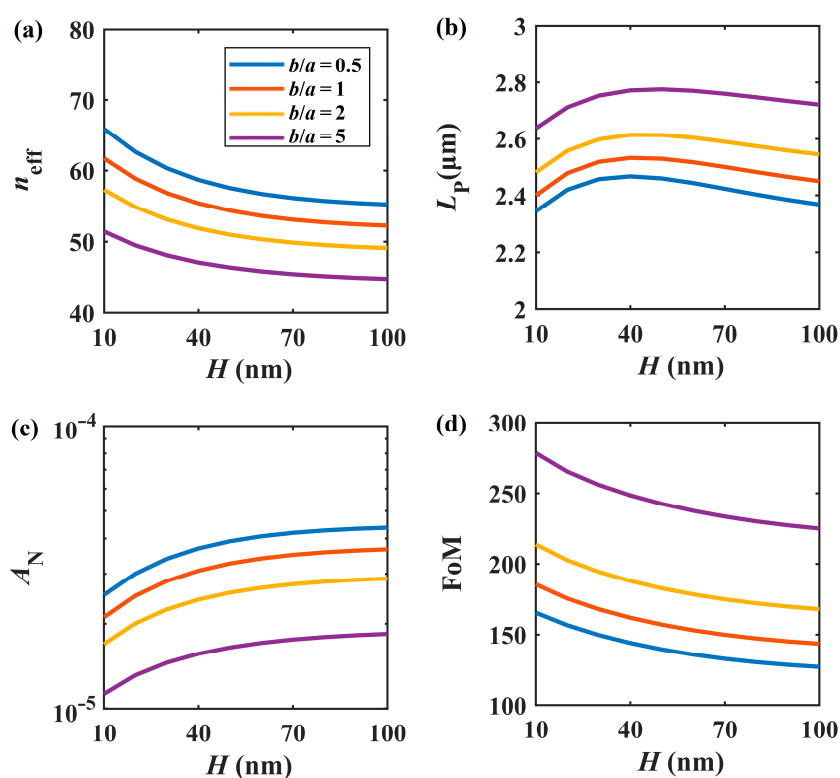
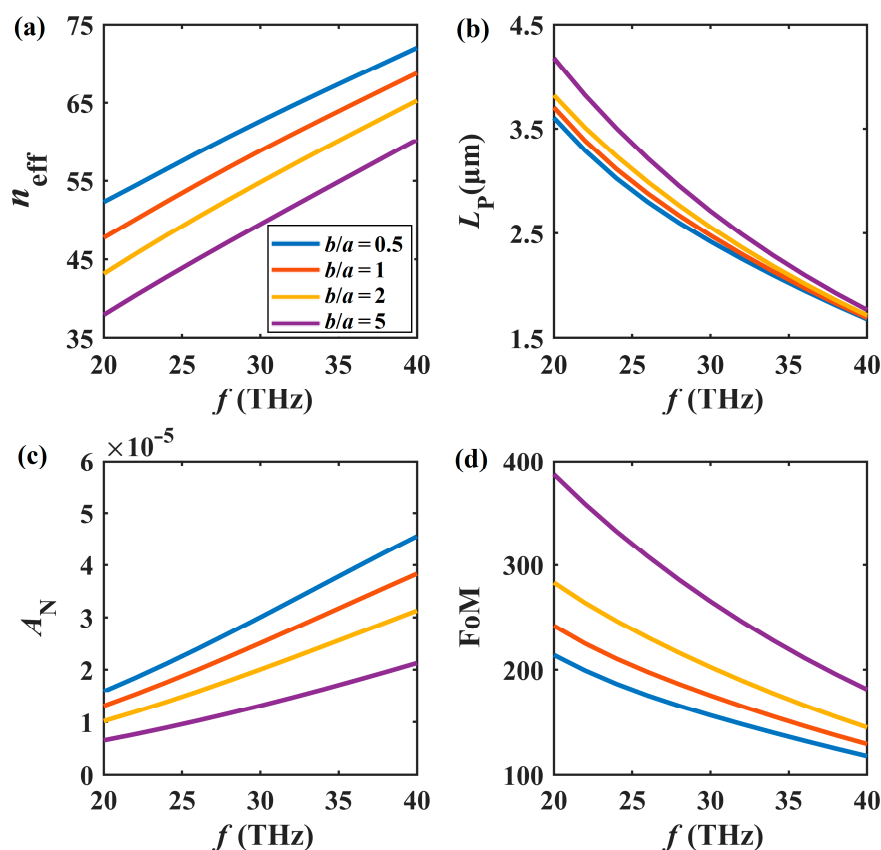


Figure 4. Modal properties of  $H$  at different  $b/a$  values. (a)  $n_{\text{eff}}$ , (b)  $L_P$ , (c)  $A_N$ , (d) FoM.

The frequency-dependent mode characteristics of the SGPWG are shown in Figure 5 at different  $b/a$  values. We set  $a = 50$  nm,  $W = 400$  nm,  $H = 20$  nm,  $h = 5$  nm, and  $E_F = 0.5$  eV. As shown in Figure 5a,b, when the frequency varies from 20 to 40 THz,  $n_{\text{eff}}$  increases linearly and  $L_P$  decreases monotonically. This is because at higher frequencies, the large absorption of graphene leads to the increase in propagation loss. From Figure 5c, we see that the normalized mode field area ( $A_N$ ) increases with increasing frequency, maintaining a level of  $\sim 10^{-5}$ . As for the figure of merit shown in Figure 5d, increasing frequency degenerates the overall performance. In other words, higher frequencies lead to higher  $n_{\text{eff}}$  and  $A_N$  values, but lower  $L_P$  and FoM values. Once again, we showed that  $b/a > 1$  settings (orange and purple lines) perform better than  $b/a = 1$  (red lines) and  $0.5$  (blue lines) settings in terms of  $L_P$ ,  $A_N$ , and FoM.

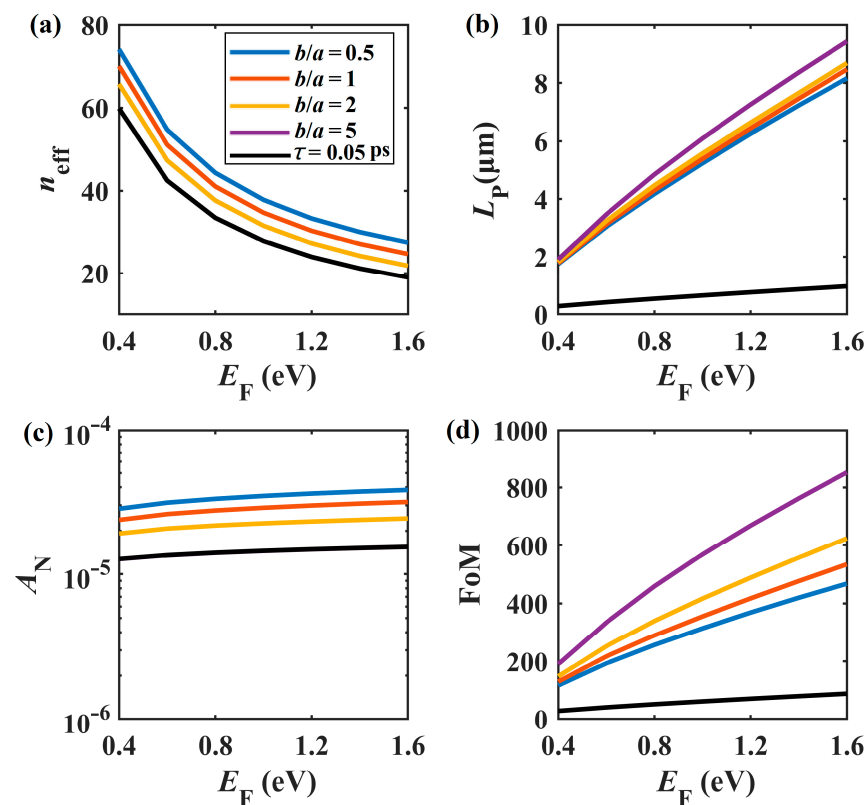


**Figure 5.** Modal properties of  $f$  at different  $b/a$  values. (a)  $n_{\text{eff}}$ , (b)  $L_P$ , (c)  $A_N$ , (d) FoM.

To present the tunability of the GP mode in the proposed SGPWG, the mode properties versus  $E_F$  are presented in Figure 6. In [65], the chemical potential of graphene could reach a value of 1.77 eV; thus,  $E_F$  varied from 0.4 to 1.6 eV. The other parameters were  $a = 50$  nm,  $W = 400$  nm,  $H = 20$  nm,  $h = 5$  nm, and  $f = 30$  THz. As shown in Figure 6a,b, when  $E_F$  changes from 0.4 to 1.6 eV, both  $n_{\text{eff}}$  and modal loss decrease monotonically. The latter is due to the fact that when the chemical potential is increased, the interband contribution of  $\sigma_g$  is drastically reduced, thus leading to the reduction of propagation loss. However, the chemical potential seems to have a limited effect on  $A_N$  (see Figure 6c), since the modal field area changes a little. In addition, the figure of merit shown in Figure 6d increases rapidly with  $E_F$  increase, and reaches a value of 850 when  $E_F = 1.6$  eV and  $b/a = 5$ . Overall, when  $b/a$  ranges from 0.5 to 5,  $L_P$  and FoM increase and  $A_N$  decreases, indicating that the elliptical nanowire-based SGPWG performs better than its circular counterparts. A recent report showed that the graphene samples fabricated by large scale methods show a relaxation time of only  $\tau = 0.05$  ps [66]. Hence, we also studied the modal properties when  $\tau = 0.05$  ps (see black lines) and  $b/a = 5$  for comparison. As seen in Figure 6b,  $L_P$  substantially decreases while  $n_{\text{eff}}$  and  $A_N$  are nearly unchanged (see Figure 6a,c), and the black lines are overlapped with the purple lines. These results indicate that the shorter relaxation time degenerates the overall performance of the SGPWG (see Figure 6d). This is because the imaginary part of the equivalent relative permittivity of monolayer graphene increases about ten times.

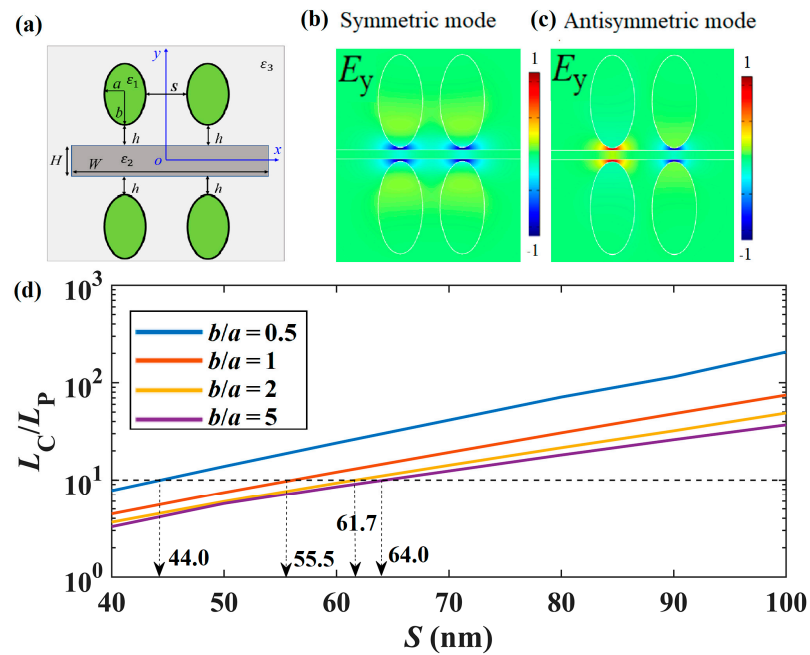
If ultra-compact photonic integration is attempted, highly localized modal fields could help reduce the crosstalk between neighboring structures. Here, we studied the crosstalk between neighboring structures by considering a system consisting of two parallel SGPWGs with an edge-to-edge distance of  $S$  (40~100 nm) as shown in Figure 7a. The parameters were  $a = 50$  nm,  $W = 800$  nm,  $H = 20$  nm,  $h = 5$  nm,  $E_F = 0.5$  eV, and  $f = 30$  THz. The electric field ( $E_y$ ) distributions of the symmetric and antisymmetric modes are depicted in

Figure 7b,c with  $S = 40$  nm and  $b/a = 2$ . Based on the coupled mode theory, the crosstalk is estimated by the coupling length  $L_C$ , which is the length required for complete power transfer from one waveguide to the other, and is given by  $L_C = \lambda_0 / (2 |n_{\text{eff},s} - n_{\text{eff},as}|)$ , where  $n_{\text{eff},s}$  and  $n_{\text{eff},as}$  denote the real parts of the effective mode indices of the symmetric and antisymmetric modes, respectively [7]. Figure 7d shows the normalized coupling lengths ( $L_C/L_P$ ) with respect to  $S$  for different  $b/a$  values. Usually, when  $L_C/L_P$  approaches 10 (see the black dashed line), it is assumed that no coupling happens between the neighboring components. When  $L_C/L_P$  reaches 10, the corresponding edge-to-edge distance are about 44.0, 55.5, 61.7, and 64.0 nm for  $b/a = 0.5, 1, 2,$  and  $5$ , respectively. It is worth noting that when  $S$  is above 64 nm,  $L_C/L_P$  is always larger than 10, which indicates that the proposed SGPWG shows extremely low crosstalk between neighboring components and is suitable for ultra-compact photonics integration.



**Figure 6.** Modal properties of  $E_F$  at different  $b/a$  values. (a)  $n_{\text{eff}}$ , (b)  $L_P$ , (c)  $A_N$ , (d) FoM. Note that the black lines overlap the purple lines in (a) and (c).

Next, we briefly compare the mode characteristics among three different kinds of waveguides, including circular nanowire-based SGPWGs with  $R = a$  (Waveguide A) and  $R = b$  (Waveguide C), and an elliptical nanowire-based SGPWG (Waveguide B). The schematics of the three SGPWGs are shown in Figure 8a, and we set  $a = 50$  nm,  $b = 150$  nm,  $W = 400$  nm,  $h = 5$  nm,  $H = 20$  nm,  $E_F = 0.5$  eV, and  $f = 30$  THz. Figure 8b shows the 2D energy density distributions of the fundamental mode in three SGPWGs. The results show that Waveguide B exhibits much stronger energy confinement than Waveguides A and C, which can be intuitively seen from Table 1 (lower  $A_N$ ). As shown in Table 1, the plasmon mode in Waveguide B has the smallest normalized mode area and largest  $L_P$  compared with the other waveguides.



**Figure 7.** Crosstalk between SGPWGs. (a) Coupling system; (b) and (c) for normalized  $E_y$  field distributions of symmetric and antisymmetric modes when  $b/a = 2$  and  $S = 40$  nm; (d)  $L_C/L_P$  with respect to  $S$  for different  $b/a$  values.

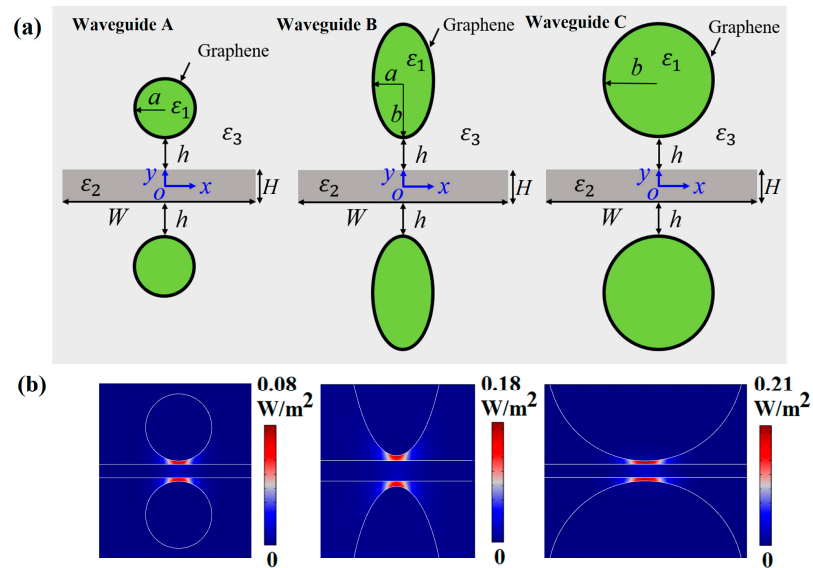


**Figure 8.** Comparison of three SGPWGs. (a) Cross-section of Waveguide A ( $R = a = 50$  nm), B ( $a = 50$  nm,  $b = 150$  nm), and C ( $R = b = 150$  nm); (b) 2D energy density distributions of (a).

**Table 1.** Waveguiding performance comparison of three SGPWGs.

Waveguide	$N_{\text{eff}}$	$L_p/\mu\text{m}$	$A_N$
A	$58.845 + 0.642i$	2.477	$2.512 \times 10^{-5}$
B	$52.428 + 0.608i$	2.616	$1.699 \times 10^{-5}$
C	$65.394 + 0.658i$	2.417	$3.501 \times 10^{-5}$

Finally, we briefly introduce the fabrication process of the SGPWG. Recent reports [67,68] showed that graphene-coated elliptical nanowires can be experimentally made by coating a dielectric nanowire with a monolayer of graphene due to van der Waals forces. Then, based on modern semiconductor fabrication technology, the substrate silica can be deposited on top of the buffer layer [69]. After that, one GCNW is placed on the silica substrate, then the GCNW is covered by silica deposition with a thickness of  $2b + h$ . Next, a silicon layer with a thickness of  $H$  (about 10 nm) could be deposited on top of the silica using plasma-enhanced chemical vapor deposition (PECVD) technology [70]. Then,  $h$ -thick silica is deposited on the silicon layer before transferring another GCNW. Finally, the second GCNW is covered by silica deposition with a thickness of over  $2b$ .

#### 4. Conclusions

In summary, a symmetric graphene plasmon waveguide is proposed and investigated. The simulation results show that a normalized mode field area of  $\sim 10^{-5}$  and a figure of merit of  $\sim 400$  can be achieved by optimizing the parameters. The mode characteristics could be dynamically tuned by changing the chemical potential of graphene by a DC bias voltage or chemical doping. By varying the ratio of  $b/a$ , the simulation results show that elliptical nanowire-based SGPWGs ( $b/a > 1$ ) show better performance compared with the cases of  $b/a \leq 1$  in terms of  $L_P$ ,  $A_N$ , and FoM. In addition, crosstalk analysis suggests that the proposed SGPWGs have extremely small energy couplings between neighboring components, even at a separation distance of 64 nm. These findings could have potential applications for ultra-compact photonic integration and subwavelength optoelectronic devices in the mid-infrared band.

**Author Contributions:** Conceptualization, D.T.; writing—original draft preparation, D.T.; Y.W.; writing—review and editing, Y.W.; T.X.; visualization, H.W.; Q.S.; supervision, D.T.; Y.T. All authors have read and agreed to the published version of the manuscript.

**Funding:** This work was supported by the Key Scientific Research Project of Henan College (21A140029), the Young Backbone Teacher Training Program of Zhengzhou Normal University (QNGG-20774), the Open Research Fund of Zhengzhou Normal University, and the Scientific Research Starting Foundation of Zhengzhou Normal University.

**Institutional Review Board Statement:** Not applicable.

**Informed Consent Statement:** Not applicable.

**Data Availability Statement:** The data presented in this study are available on request from the corresponding author.

**Conflicts of Interest:** The authors declare no conflict of interest.

#### References

1. Oulton, R.F.; Sorger, V.J.; Genov, D.A.; Pile, D.F.P.; Zhang, X. A hybrid plasmonic waveguide for subwavelength confinement and long-range propagation. *Nat. Photon.* **2008**, *2*, 496–500. [[CrossRef](#)]
2. Cheben, P.; Halir, R.; Schmid, J.H.; Atwater, H.A.; Smith, D.R. Subwavelength integrated photonics. *Nature* **2018**, *560*, 565–572. [[CrossRef](#)]
3. Verhagen, E.; Polman, A.; Kuipers, L.K. Nanofocusing in laterally tapered plasmonic waveguides. *Opt. Express* **2008**, *16*, 45–57. [[CrossRef](#)] [[PubMed](#)]
4. Yang, L.; Li, P.; Li, Z. Plasmonic polarization beam splitting based on single silver nanowire. *Opt. Express* **2019**, *27*, 3851–3860. [[CrossRef](#)] [[PubMed](#)]
5. Lu, F.; Zhang, W.; Huang, L.; Liang, S.; Mao, D.; Gao, F.; Mei, T.; Zhao, J. Mode evolution and nanofocusing of grating-coupled surface plasmon polaritons on metallic tip. *Opto-Electron. Adv.* **2018**, *1*, 180010. [[CrossRef](#)]
6. Moreno, E.; Rodrigo, S.G.; Bozhevolnyi, S.I.; Martín-Moreno, L.; García-Vidal, F.J. Guiding and focusing of electromagnetic fields with wedge plasmon polaritons. *Phys. Rev. Lett.* **2008**, *100*, 023901. [[CrossRef](#)] [[PubMed](#)]
7. Veronis, G.; Fan, S. Crosstalk between three-dimensional plasmonic slot waveguides. *Opt. Express* **2008**, *16*, 2129–2140. [[CrossRef](#)]
8. Gao, H.; Cao, Q.; Zhu, M.; Teng, D.; Shen, S. Nanofocusing of terahertz wave in a tapered hyperbolic metal waveguide. *Opt. Express* **2014**, *22*, 32071–32081. [[CrossRef](#)]

9. Zhang, Q.; Hao, H.; Ren, J.; Zhang, F.; Gong, Q.; Gu, Y. A quantum phase gate capable of effectively collecting photons based on a gap plasmon structure. *Nanoscale* **2020**, *12*, 10082–10089. [[CrossRef](#)]
10. Steinberger, B.; Hohenau, A.; Ditzbacher, H.; Stepanov, A.L.; Drezet, A.; Aussenegg, F.R.; Leitner, A.; Krenn, J.R. Dielectric stripes on gold as surface plasmon waveguides. *Appl. Phys. Lett.* **2006**, *88*, 094104. [[CrossRef](#)]
11. Krasavin, A.V.; Zayats, A.V. Three-dimensional numerical modeling of photonic integration with dielectric-loaded SPP waveguides. *Phys. Rev. B* **2008**, *78*, 045425. [[CrossRef](#)]
12. Han, Z.; Radko, I.P.; Mazurski, N.; Desiatov, B.; Beermann, J.; Albrechtsen, O.; Levy, U.; Bozhevolnyi, S.I. On-chip detection of radiation guided by dielectric-loaded plasmonic waveguides. *Nano Lett.* **2015**, *15*, 476–480. [[CrossRef](#)] [[PubMed](#)]
13. Dai, D.; He, S. A silicon-based hybrid plasmonic waveguide with a metal cap for a nano-scale light confinement. *Opt. Express* **2009**, *17*, 16646–16653. [[CrossRef](#)]
14. Chen, L.; Zhang, T.; Li, X.; Huang, W. Novel hybrid plasmonic waveguide consisting of two identical dielectric nanowires symmetrically placed on each side of a thin metal film. *Opt. Express* **2012**, *20*, 20535–20544. [[CrossRef](#)] [[PubMed](#)]
15. Alam, M.Z.; Aitchison, J.S.; Mojahedi, M. A marriage of convenience: Hybridization of surface plasmon and dielectric waveguide modes. *Laser Photonics Rev.* **2014**, *8*, 394–408. [[CrossRef](#)]
16. Zhang, L.; Pan, C.; Zeng, D.; Yang, Y.; Yang, Y.; Junxian, M. A hybrid-plasmonic-waveguide-based polarization-independent directional coupler. *IEEE Access* **2020**, *8*, 134268–134275. [[CrossRef](#)]
17. Teng, D.; Cao, Q.; Wang, K. An extension of the generalized nonlocal theory for the mode analysis of plasmonic waveguides at telecommunication frequency. *Journal of Optics* **2017**, *19*, 055003. [[CrossRef](#)]
18. Tuniz, A.; Bickerton, O.; Diaz, F.J.; Kasebier, T.; Kley, E.B.; Kroker, S.; Palomba, S.; de Sterke, C.M. Modular nonlinear hybrid plasmonic circuit. *Nat. Commun.* **2020**, *11*, 2413. [[CrossRef](#)] [[PubMed](#)]
19. Huang, T.J.; Yin, L.Z.; Zhao, J.; Du, C.H.; Liu, P.K. Amplifying evanescent waves by dispersion-induced plasmons: Defying the materials limitation of superlens. *ACS Photonics* **2020**, *7*, 2173–2181. [[CrossRef](#)]
20. Gao, Y.; Shadrivov, I.V. Second harmonic generation in graphene-coated nanowires. *Opt. Lett.* **2016**, *41*, 3623–3626. [[CrossRef](#)] [[PubMed](#)]
21. Barnes, W.L.; Dereux, A.; Ebbesen, T.W. Surface plasmon subwavelength optics. *Nature* **2003**, *424*, 824–830. [[CrossRef](#)]
22. Novoselov, K.S.; Fal, V.I.; Colombo, L.; Gellert, P.R.; Schwab, M.G.; Kim, K. A roadmap for graphene. *Nature* **2012**, *490*, 192–200. [[CrossRef](#)] [[PubMed](#)]
23. Fan, Y.C.; Shen, N.H.; Zhang, F.L.; Zhao, Q.; Wu, H.J.; Fu, Q.H.; Wei, Z.Y.; Li, H.Q.; Soukoulis, C.M. Graphene plasmonics: A platform for 2D Optics. *Adv. Opt. Mater.* **2019**, *7*, 1800537. [[CrossRef](#)]
24. Teng, D.; Wang, K.; Li, Z. Graphene-coated nanowire waveguides and their applications. *Nanomaterials* **2020**, *10*, 229. [[CrossRef](#)] [[PubMed](#)]
25. Zheng, K.; Yuan, Y.F.; He, J.J.; Gu, G.Q.; Zhang, F.; Chen, Y.; Song, J.; Qu, J.L. Ultra-high light confinement and ultra-long propagation distance design for integratable optical chips based on plasmonic technology. *Nanoscale* **2019**, *11*, 4601–4613. [[CrossRef](#)]
26. Shan, H.; Yu, Y.; Wang, X.; Luo, Y.; Zu, S.; Du, B.; Han, T.Y.; Li, B.W.; Li, Y.; Wu, J.R.; et al. Fang, Z. Direct observation of ultrafast plasmonic hot electron transfer in the strong coupling regime. *Light Sci. Appl.* **2019**, *8*, 9. [[CrossRef](#)] [[PubMed](#)]
27. He, X.; Liu, F.; Lin, F.; Xiao, G.; Shi, W. Tunable MoS<sub>2</sub> modified hybrid surface plasmon waveguides. *Nanotechnology* **2018**, *30*, 125201. [[CrossRef](#)] [[PubMed](#)]
28. Jiang, Y.; Shi, C.; Wang, J. A hybrid plasmonic terahertz waveguide with ridge structure base on Bulk-Dirac-semimetal. *Opt. Commun.* **2020**, *475*, 126239. [[CrossRef](#)]
29. He, X.; Liu, F.; Lin, F.; Lin, F.; Shi, W. Tunable 3D Dirac-semimetals supported Mid-IR hybrid plasmonic waveguides. *Opt. Lett.* **2021**, *46*, 472–475. [[CrossRef](#)]
30. Dereshgi, S.A.; Liu, Z.; Aydin, K. Anisotropic localized surface plasmons in borophene. *Opt. Express* **2020**, *28*, 16725–16739. [[CrossRef](#)] [[PubMed](#)]
31. Lian, C.; Hu, S.Q.; Zhang, J.; Cheng, C.; Yuan, Z.; Gao, S.; Meng, S. Integrated plasmonics: Broadband dirac plasmons in borophene. *Phys. Rev. Lett.* **2020**, *125*, 116802. [[CrossRef](#)] [[PubMed](#)]
32. Wang, J.; Xing, Z.; Chen, X.; Cheng, Z.Z.; Li, X.J.; Liu, T. Recent progress in waveguide-integrated graphene photonic devices for sensing and communication applications. *Front. Phys.* **2020**, *8*, 37. [[CrossRef](#)]
33. Yu, P.; Fesenko, V.I.; Tuz, V.R. Dispersion features of complex waves in a graphene-coated semiconductor nanowire. *Nanophotonics* **2018**, *7*, 925–934. [[CrossRef](#)]
34. Saeed, M.; Ghaffar, A.; Alkanhal, M.A.S.; Alqahtani, A.H.; Khan, Y.; ur Rehman, S. Plasmon modes supported by metamaterial-filled monolayer graphene cylindrical waveguides. *J. Opt. Soc. Am. B* **2020**, *37*, 3515–3525. [[CrossRef](#)]
35. Xing, R.; Jian, S. Numerical analysis on the multilayer nanoring waveguide pair. *IEEE Photon. Technol. Lett.* **2016**, *28*, 2779–2782. [[CrossRef](#)]
36. Teng, D.; Wang, K.; Li, Z.; Zhao, Y. Graphene-coated nanowire dimers for deep subwavelength waveguiding in mid-infrared range. *Opt. Express* **2019**, *27*, 12458–12469. [[CrossRef](#)]
37. Wu, D.; Tian, J. Study on the plasmonic characteristics of bow-tie type graphene-coated nanowire pair. *Optik* **2018**, *156*, 689–695. [[CrossRef](#)]

38. Wang, X.; Wang, J.; Ma, T.; Liu, H.; Wang, F. Plasmonic characteristics of suspended graphene-coated wedge porous silicon nanowires with Ag partition. *Chin. Phys. B* **2021**, *30*, 014207. [[CrossRef](#)]
39. Teng, D.; Wang, K. Theoretical analysis of terahertz dielectric-loaded graphene waveguide. *Nanomaterials* **2021**, *11*, 210. [[CrossRef](#)] [[PubMed](#)]
40. Jabbarzadeh, F.; Habibzadeh-Sharif, A. High performance dielectric loaded graphene plasmonic waveguide for refractive index sensing. *Opt. Commun.* **2021**, *479*, 126419. [[CrossRef](#)]
41. Zhu, J.; Jiang, F.; Yunbai, Q. Sense of surface plasmon polarization waveguide of graphene. *Plasmonics* **2019**, *14*, 1903–1910. [[CrossRef](#)]
42. Liao, B.; Guo, X.; Hu, H.; Liu, N.; Chen, K.; Yang, X.; Dai, Q. Ultra-compact graphene plasmonic filter integrated in a waveguide. *Chin. Phys. B* **2018**, *27*, 094101. [[CrossRef](#)]
43. Xu, Y.; Li, F.; Kang, Z.; Huang, D.; Zhang, X.; Tam, H.-Y.; Wai, P.K.A. Hybrid graphene-silicon based polarization-insensitive electro-absorption modulator with high-modulation efficiency and ultra-broad bandwidth. *Nanomaterials* **2019**, *9*, 157. [[CrossRef](#)]
44. Hao, R.; Jiao, J.; Peng, X.; Zhen, Z.; Dagarbek, R.; Zou, Y.; Li, E. Experimental demonstration of a graphene-based hybrid plasmonic modulator. *Opt. Lett.* **2019**, *44*, 2586–2587. [[CrossRef](#)] [[PubMed](#)]
45. Liu, J.P.; Zhai, X.; Xie, F.; Wang, L.L.; Xia, S.X.; Li, H.J.; Luo, X.; Shang, X.J. Analytical model of mid-infrared surface plasmon modes in a cylindrical long-range waveguide with double-layer graphene. *J. Lightwave Technol.* **2017**, *35*, 1971–1979. [[CrossRef](#)]
46. Hajati, M.; Hajati, Y. Investigation of plasmonic properties of graphene multilayer nano-ribbon waveguides. *Appl. Opt.* **2016**, *55*, 1878–1884. [[CrossRef](#)] [[PubMed](#)]
47. Wang, Y.; Liu, H.; Wang, S.; Cai, M.; Ma, L. Optical transport properties of graphene surface plasmon polaritons in mid-infrared band. *Crystals* **2019**, *9*, 354. [[CrossRef](#)]
48. Ctyroky, J.; Petrák, J.; Kuzmiak, V.; Kwicien, P.; Richter, I. Silicon waveguides with graphene: Coupling of waveguide mode to surface plasmons. *J. Opt.* **2020**, *22*, 095801. [[CrossRef](#)]
49. Chen, X.; Wang, Y.; Xiang, Y.; Jiang, G.; Wang, L.; Bao, Q.; Zhang, H.; Liu, Y.; Wen, S.; Fan, D. A broadband optical modulator based on a graphene hybrid plasmonic waveguide. *J. Lightwave Technol.* **2016**, *34*, 4948–4953. [[CrossRef](#)]
50. Hasan, K.B.M.R.; Islam, M.A.; Alam, M.S. Design of a broadband single mode hybrid plasmonic waveguide incorporating silicon nanowire. *Opt. Mater. Express* **2020**, *10*, 2783–2799. [[CrossRef](#)]
51. Hajati, M.; Hajati, Y. High-performance and low-loss plasmon waveguiding in graphene-coated nanowire with substrate. *J. Opt. Soc. Am. B* **2016**, *33*, 2560–2565. [[CrossRef](#)]
52. Hajati, M.; Hajati, Y. Plasmonic characteristics of two vertically coupled graphene-coated nanowires integrated with substrate. *Appl. Opt.* **2017**, *56*, 870–875. [[CrossRef](#)]
53. Sun, M.; Tian, J.; Lan, X.; He, Z.; Liu, J. Transmission properties of two vertically coupled double-graphene-coated nanowires integrated with substrate. *Optik* **2019**, *185*, 242–247. [[CrossRef](#)]
54. Teng, D.; Guo, J.; Yang, Y.; Ma, W.; Wang, K. Study of modal properties in graphene-coated nanowires integrated with substrates. *Appl. Phys. B* **2020**, *126*, 173. [[CrossRef](#)]
55. Teng, D.; Yang, Y.; Guo, J.; Ma, W.; Tang, Y.; Wang, K. Efficient guiding mid-infrared waves with graphene-coated nanowire based plasmon waveguides. *Res. Phys.* **2020**, *17*, 103169. [[CrossRef](#)]
56. Teng, D.; Wang, K.; Huan, Q.; Chen, W.; Li, Z. High-performance light transmission based on graphene plasmonic waveguides. *J. Mater. Chem. C* **2020**, *8*, 6832–6838. [[CrossRef](#)]
57. Chandler-Horowitz, D.; Amirtharaj, P.M. High-accuracy, midinfrared ( $450\text{ cm}^{-1} \leq \omega \leq 4000\text{ cm}^{-1}$ ) refractive index values of silicon. *J. Appl. Phys.* **2005**, *97*, 123526. [[CrossRef](#)]
58. Yang, X.; Liu, X.; Yu, S.; Gan, L.; Zhou, J.; Zeng, Y. Permittivity of undoped silicon in the millimeter wave range. *Electronics* **2019**, *8*, 886. [[CrossRef](#)]
59. Yu, H.; Wang, H.; Xiong, Q.; Mei, J.; Zhang, Y.; Wang, Y.; Lai, J.; Chen, C. Photothermal switch of sub-microsecond response: A monolithic-integrated ring resonator and a metasurface absorber in silicon photonic crystals. *Opt. Lett.* **2020**, *45*, 1806–1809.
60. Ono, M.; Hata, M.; Tsunekawa, M.; Nozaki, K.; Sumikura, H.; Chiba, H.; Notomi, M. Ultrafast and energy-efficient all-optical switching with graphene-loaded deep-subwavelength plasmonic waveguides. *Nat. Photon.* **2020**, *14*, 37–43. [[CrossRef](#)]
61. Nikitin, A.Y.; Alonso-González, P.; Hillenbrand, R. Efficient coupling of light to graphene plasmons by compressing surface polaritons with tapered bulk materials. *Nano Lett.* **2014**, *14*, 2896–2901. [[CrossRef](#)] [[PubMed](#)]
62. Buckley, R.; Berini, P. Figures of merit for 2D surface plasmon waveguides and application to metal stripes. *Opt. Express* **2007**, *15*, 12174–12182. [[CrossRef](#)] [[PubMed](#)]
63. Said, A.; Atia, K.S.R.; Obayya, S.S.A. On modeling of plasmonic devices: Overview. *J. Opt. Soc. Am. B* **2020**, *37*, A163–A174. [[CrossRef](#)]
64. Caridad, J.M.; Winters, S.; McCloskey, D.; Duesberg, G.S.; Donegan, J.F.; Krstić, V. Hot-volumes as uniform and reproducible sers-detection enhancers in weakly-coupled metallic nanohelices. *Sci. Rep.* **2017**, *7*, 45548. [[CrossRef](#)]
65. Kanahashi, K.; Tanaka, N.; Shoji, Y.; Maruyama, M.; Jeon, I.; Kawahara, K.; Ishihara, M.; Hasegawa, M.; Ohta, H.; Ago, H.; et al. Formation of environmentally stable hole-doped graphene films with instantaneous and high-density carrier doping via a boron-based oxidant. *npj 2D Mater. Appl.* **2019**, *3*, 44. [[CrossRef](#)]
66. Whelan, P.R.; Shen, Q.; Zhou, B.; Serrano, I.G.; Kamalakar, M.V.; Mackenzie, D.M.; Ji, J.; Huang, D.; Shi, H.; Luo, D.; et al. Fermi velocity renormalization in graphene probed by terahertz time-domain spectroscopy. *2D Mater.* **2020**, *7*, 035009. [[CrossRef](#)]

67. Cao, T.; Li, Y.; Tian, L.; Liang, H.; Qin, K. Fast switching “On/Off” chiral surface plasmon polaritons in graphene-coated Ge<sub>2</sub>Sb<sub>2</sub>Te<sub>5</sub> nanowire. *ACS Appl. Nano Mater.* **2018**, *1*, 759–767. [[CrossRef](#)]
68. Chen, B.; Meng, C.; Yang, Z.; Li, W.; Lin, S.; Gu, T.; Guo, X.; Wang, D.; Yu, S.; Wong, C.W.; et al. Graphene coated ZnO nanowire optical waveguides. *Opt. Express* **2014**, *22*, 24276–24285. [[CrossRef](#)]
69. Vitanov, P.; Ivanova, T.; Dikov, H. Low-temperature deposition of ultrathin SiO<sub>2</sub> films on Si substrates. *J. Phys. Conf. Ser.* **2014**, *514*, 012010. [[CrossRef](#)]
70. Flöry, N.; Ma, P.; Salamin, Y.; Emboras, A.; Taniguchi, T.; Watanabe, K.; Leuthold, J.; Novotny, L. Waveguide-integrated van der Waals heterostructure photodetector at telecom wavelengths with high speed and high responsivity. *Nat. Nanotechnol.* **2020**, *15*, 118–124. [[CrossRef](#)]